

## 7 Evidence for the Onset of Three-Body Decay in Photodissociation of Vibrationally Excited $\text{CHFCl}_2$

Excitation of C-H stretch overtones of  $\text{CHFCl}_2$  followed by  $\sim 235$  nm photodissociation was applied to investigate the effect of internal parent excitation on the dynamics of two- and three-body photofragmentation. The  $\sim 235$  nm photons also tagged ground  $\text{Cl } ^2\text{P}_{3/2}$  [ $\text{Cl}$ ] and spin-orbit excited  $\text{Cl } ^2\text{P}_{1/2}$  [ $\text{Cl}^*$ ] state photofragments, via (2+1) resonance enhanced multiphoton ionization (REMPI) in a time-of-flight (TOF) mass spectrometer, and monitored their time-of-arrival profiles. These profiles revealed the product velocities and angular distributions of  $^{35}\text{Cl}$  and  $^{35}\text{Cl}^*$  and suggest the contribution of three-body decay in photodissociation of  $\text{CHFCl}_2$  pre-excited with five quanta of C-H stretch. This is the first evidence for three-body decay in photodissociation of vibrationally excited molecules.

### 7.1 Introduction

Vibrationally mediated photodissociation (VMP),<sup>1</sup> in which molecules are prepared in a vibrationally excited state and then promoted by a photon to a dissociative excited state, is now recognized as a method that provides direct means for studying the influence of rovibrational excitation on dynamics. The VMP approach was applied to several molecular systems including water isotopomers,<sup>2-6</sup>  $\text{HNCO}$ ,<sup>7</sup>  $\text{C}_2\text{H}_2$ ,<sup>8,9</sup>  $\text{C}_2\text{HD}$ ,<sup>10</sup>  $\text{CD}_3\text{C}\equiv\text{CH}$ ,<sup>11</sup>  $\text{CH}_3\text{Cl}$  and  $\text{CHD}_2\text{Cl}$ ,<sup>12</sup>  $\text{HN}_3$ ,<sup>13</sup>  $\text{CH}_3\text{CFC}_2$ ,<sup>14,15</sup> and  $\text{CHFCl}_2$ .<sup>16</sup> These studies revealed the effect of the initial state preparation on relative yields of product channels, on internal state distributions and on vector correlations. In particular, in some cases alteration of product identity or distribution in VMP could be found in comparison to the almost isoenergetic one-photon photodissociation.<sup>7,8,11,12,14,15</sup> This is due to sampling of different portions of the upper potential energy surfaces (PESs) by the vibrationally excited wavefunction and as a result of the participation of more than one PES leading to different adiabatic and nonadiabatic interplay in VMP compared to the one-photon photodissociation.

In view of the impact of vibrational pre-excitation on two-body photodissociation processes it is expected that three-body break-up of molecules, where molecules split into three fragments, might be affected as well. As stated recently,<sup>17,18</sup> three-body decays are of

much importance in atmospheric and combustion processes, but nevertheless represent an almost unexplored field of chemical reaction dynamics. Therefore, studies that test the effect of initial parent nuclear motion on the three-body fragmentation, although of high complexity, might provide new insight into these processes and an understanding of bond breaking. Of particular interest in three-body dissociation is the energy disposal among the emerging fragments that might shed light on the involved PESs and the ensuing dynamics during dissociation.

The molecule chosen to test the plausibility of three-body breakup in VMP is  $\text{CHFCl}_2$ . This hydrochlorofluorocarbon (HCFC) compound, like other HCFCs, is of atmospheric relevance due to its use as interim replacement for the ozone destroying chlorofluorocarbons (CFCs) and halons. Various aspects of the photolysis of  $\text{CHFCl}_2$  (HCFC-21) received previously some attention. Rebbert et al.<sup>19</sup> photodissociated  $\text{CHFCl}_2$  at 213.9, 163.3 and 147 nm at room temperature in the presence of radical scavengers ( $\text{CH}_4$ ,  $\text{Br}_2$ ,  $\text{HBr}$ , and  $\text{HCl}$ ). They found that for the first two wavelengths the primary process is C-Cl bond cleavage, while at the shorter wavelength the resulting  $\text{CHFCl}$  radicals further decompose to produce  $\text{HCl}$  and  $\text{CF}$ . Similarly, Hauteclouque<sup>20</sup> photodissociated  $\text{CHFCl}_2$  in the 170–190 nm range and found that the predominant channel is Cl formation, but they also found appreciable yields of the molecular fragments  $\text{HCl}$  and  $\text{Cl}_2$ . More recently, dynamical studies under collision free conditions were carried out to observe the major pathway of loss of one chlorine atom<sup>16,21</sup> and the minor release of hydrogen photofragments.<sup>16</sup>

The study of C-Cl bond rupture in photodissociation of vibrationless ground state  $\text{CHFCl}_2$  molecules at 193 nm ( $51\,813\text{ cm}^{-1}$ ) was performed by Huber and co-workers<sup>21</sup> using the method of photofragment translational spectroscopy (PTS). They revealed the kinetic energy release and a positive anisotropy ( $\beta = 0.5 \pm 0.1$ ) for it. We photodissociated<sup>16</sup> jet-cooled  $\text{CHFCl}_2$  molecules excited to C-H stretch-bend polyad components<sup>22</sup> including  $N = 3$  (three C-H stretch quanta),  $N = 7/2$  (three C-H stretch quanta + a bend) and  $N = 4$  (four C-H stretch quanta) by  $\sim 235$  nm photons. These photons also tagged the spin-orbit ground  $\text{Cl } ^2\text{P}_{3/2} [\text{Cl}]$  and excited  $\text{Cl } ^2\text{P}_{1/2} [\text{Cl}^*]$  states via resonance enhanced multiphoton ionization (REMPI) in a time-of-flight mass spectrometer (TOF MS). The action spectra and the Doppler profiles of the corresponding photofragments were measured, revealing that both  $\text{Cl}$  and  $\text{Cl}^*$  are released as a result of C-Cl bond cleavage. From the area ratios of the

Doppler profiles, the branching into the Cl\* and Cl photofragments were determined with a Cl\*/Cl ratio of about one half. We also found a low fractional yield of H/[Cl + Cl\*], indicating H photofragments generation to some extent. In addition, due to the reduction of the rotational inhomogeneous broadening and of the overlap with hot bands, in the action spectra, details about the vibrational dynamics were obtained.

In this work we focus on the ~235 nm photodissociation of CHFCl<sub>2</sub> molecules prepared in the 3<sub>1</sub>, 4<sub>1</sub>, and 5<sub>1</sub> C-H stretch-bend polyad components (the subscript 1 designates the highest frequency component).<sup>16</sup> These components are mixtures of zeroth-order bright states and close lying dark states. They comprise main contributions of the former which are three, four, and five C-H stretch quanta, respectively, and some of the latter that include bends and are coupled via the 2:1 Fermi resonance. The velocities and anisotropy parameters,  $\beta$ , were obtained from the time-of-arrival profiles of <sup>35</sup>Cl and <sup>35</sup>Cl\*. The velocity distributions of both Cl and Cl\* for molecules promoted from the 5<sub>1</sub> state of CHFCl<sub>2</sub> are broader than from the 3<sub>1</sub> and 4<sub>1</sub> states reflecting the higher energy content in the former. However, the broadening does not result only from "fast" Cl and Cl\* photofragments, but also from a small fraction of "slow" photofragments, indicating the onset of three-body decay in 235 nm photodissociation of CHFCl<sub>2</sub> (5<sub>1</sub>).

## 7.2 Experiment

The experiments were carried out in a home-built Wiley-McLaren TOF MS<sup>23</sup> similar to that reported previously.<sup>14-16</sup> The experimental set-up is schematically shown in Fig. 7.1.

The CHFCl<sub>2</sub> sample (98 % purity) prepared as a 10 % mixture in Ar at a total pressure of 10<sup>3</sup> mbar, was expanded through a nozzle-skimmer arrangement. The pressure in the ionization chamber was typically ~2·10<sup>-5</sup> mbar with the molecular beam on. Under these conditions the beam is characterized by a predominant rotational temperature of about 8 K and vibrational temperature of < 100 K, as estimated from the VMP of propyne-d<sub>3</sub> (3v<sub>1</sub>).<sup>11</sup> These temperatures minimize the rotational inhomogeneous structure and the overlap with hot bands in the region of the monitored polyad components.<sup>16</sup> The source of vibrational overtone excitation (IR/visible) pulses, (~10 mJ around 1147.6 nm for preparation of 3<sub>1</sub>, ~10 mJ around 878.7 nm for 4<sub>1</sub> and ~20 mJ near 716 nm for 5<sub>1</sub>) was the idler beam of an optical parametric oscillator (bandwidth ~0.08 cm<sup>-1</sup>). Following the excitation pulse, after a

delay of  $\sim 15$  ns, the excited  $\text{CH}_2\text{FCl}$  molecules were photodissociated by a counter-propagating UV beam ( $\sim 100$   $\mu\text{J}$ ) from a frequency doubled tunable dye laser ( $0.4$   $\text{cm}^{-1}$ ).

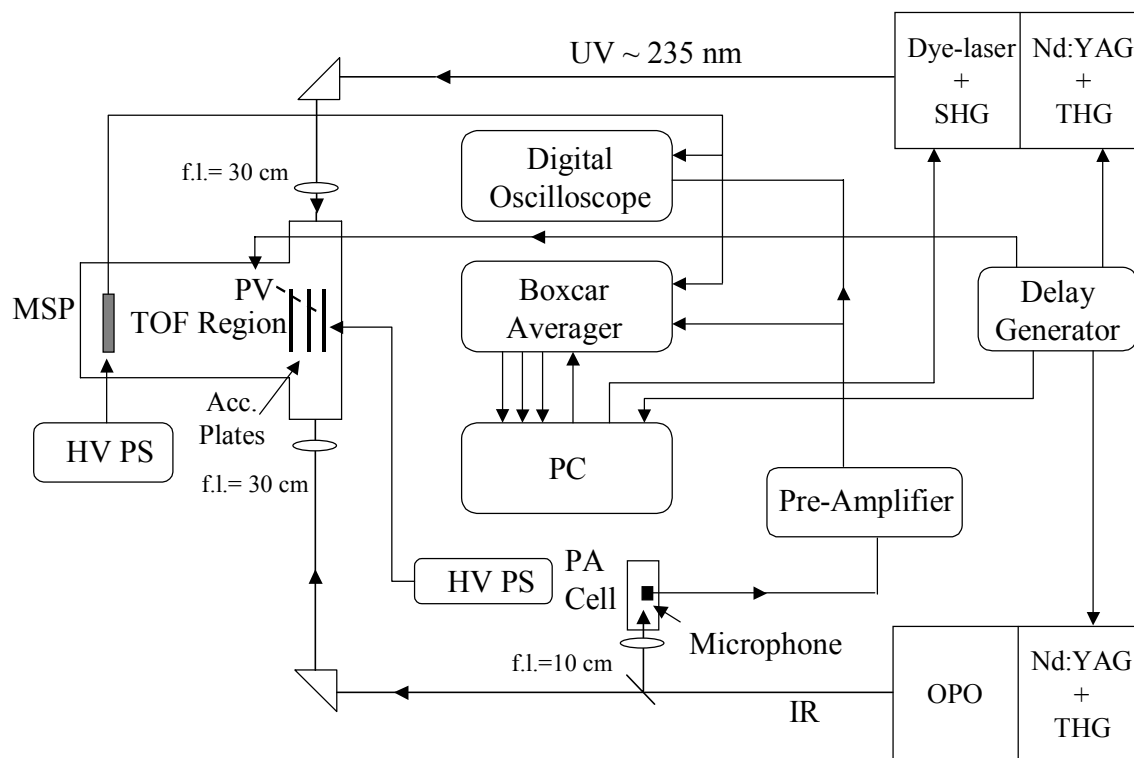


**Figure 7.1:** Schematic diagram of the experimental set-up. TOF: time-of-flight, MSP: microsphere plate, PV: pulsed valve, HV PS: high voltage power supply, SHG: second harmonic generator, THG: third harmonic generator, OPO: optical parametric oscillator, IR: overtone vibrational excitation laser beam, UV: photolysis and probe laser beam, f. l.: focal length, PA: photoacoustic, PC: personal computer.

The wavelength of this beam was chosen to fit the two-photon transition of  $\text{Cl}$  ( $4p^2D_{3/2} \leftarrow 3p^2P_{3/2}$ ) at 235.336 nm and  $\text{Cl}^*$  ( $4p^2P_{1/2} \leftarrow 3p^2P_{1/2}$ ) at 235.205 nm in order to also tag the  $\text{Cl}$  and  $\text{Cl}^*$  photofragments, respectively, by (2+1) REMPI.<sup>24</sup> The IR/visible beam was focused with a 15 cm focal length (f.l.) lens, while the photolysis/probe (UV) beam with a 30 cm f.l. lens. The UV laser photolysed the  $\text{CH}_2\text{FCl}$  molecules efficiently only when overtone excitation was induced, due to the very low absorption cross section of vibrationless ground state molecules at  $\sim 235$  nm, as shown in Fig. 7.2.<sup>25</sup>

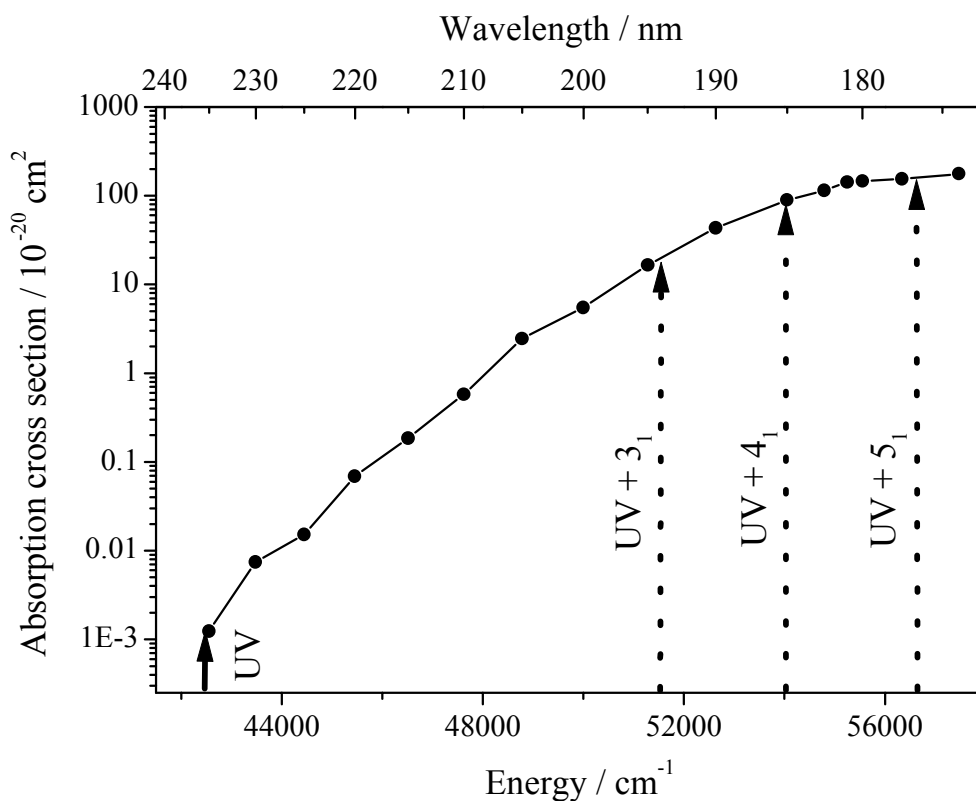


**Figure 7.2:** Logarithmic absorption cross section of  $\text{CHFCl}_2$  based on the publication of Hubrich et al.<sup>25</sup> The combined wavelengths (IR + UV) used in the present experiment are marked by dotted arrows, whereas the ground state photodissociation wavelength is marked by a solid arrow. The displayed range is related to the first absorption band of HCFCs (designed as the A band) in the 180-240 nm. This band is broad and unstructured. At high energy the cross section is highly decreasing by several orders of magnitude at the red wing. The electronic transition can be described as a  $\sigma^* \leftarrow n_{\text{Cl}}$  excitation, involving the promotion of an electron from a nonbonding Cl  $2p$  orbital to an antibonding C-Cl orbital.

Ions formed via REMPI in the focal volume were subject to continuously biased extraction (-450 V), two acceleration stages (-850 V and -1700 V), two pairs of orthogonal deflection plates, and an einzel lens. The ions then entered the field-free drift region (55 cm long) and were finally detected by a microsphere plate. The time-of-arrival profiles of the  $^{35}\text{Cl}$  and  $^{35}\text{Cl}^*$  resulting from 5000 shots were recorded with a digital oscilloscope and stored on a disk for later analysis. The TOF profiles were taken under space focusing conditions<sup>23</sup> at two different geometries, vertical (UV laser polarization perpendicular to the TOF axis) and horizontal (UV laser polarization parallel to the TOF axis). The effects of the

apparatus on the time-of-arrival profiles were determined using the approach of Varley and Dagdigan,<sup>26</sup> i.e. measurement of the time-of-arrival profiles of  $^{35}\text{Cl}$  photofragments from 355 nm photolysis of  $\text{Cl}_2$ . These profiles allowed calibration of the electric field strength,  $E$ , in the ionization region, which was found to be 124 V/cm, 12 % lower than the nominal field strength. In addition, the profiles enabled to estimate the apparatus response time and the effective probe laser linewidth that affects the time-of-arrival profiles through Doppler velocity selection along the probe laser direction.<sup>26</sup>

## 7.3 Results and Discussion

### 7.3.1 Time-of-Arrival Profiles and Their Analysis

Experimental  $^{35}\text{Cl}$  and  $^{35}\text{Cl}^*$  ion arrival time profiles following the  $\sim 235$  nm photodissociation of  $\text{CHFCl}_2$  prepared in the Q-branch (comprising several unresolved rotational states) of the  $3_1$ ,  $4_1$ , and  $5_1$  vibrational states are displayed in Fig. 7.3 (a) - (c), respectively. Only the portions showing the  $^{35}\text{Cl}$  fragments are exhibited, although essentially similar distributions were also observed, at slightly longer flight times, for the  $^{37}\text{Cl}$  fragments. However, since the intensity of the signal of  $^{35}\text{Cl}$  is three times larger than that of  $^{37}\text{Cl}$ , due to its larger natural abundance, analysis of the former was preferred. These profiles represent the VMP "net" profiles, and were obtained by removing the contribution, when significant, resulting from the  $\sim 235$  nm photodissociation of vibrationless ground state molecules (vibrational excitation laser off) from the signal monitored when both the vibrational excitation laser and the UV laser were on.

The observed profiles were obtained with the polarization of the photolysis/probe UV laser parallel or perpendicular to the TOF MS axis and with the polarization of the IR/visible vibrational excitation laser axis remaining fixed with perpendicular polarization. The profiles of both  $\text{Cl}$  and  $\text{Cl}^*$ , taken under these polarization conditions, are shown in Fig. 7.3 (a) – (c). It is worth noting that profiles monitored with the polarization of the visible/IR laser parallel to the TOF MS axis were similar to those shown in Fig. 7.3. This indicates that the vibrational excitation to the Q-branch of the  $3_1$ ,  $4_1$ , and  $5_1$  states does not induce significant alignment to the molecules.

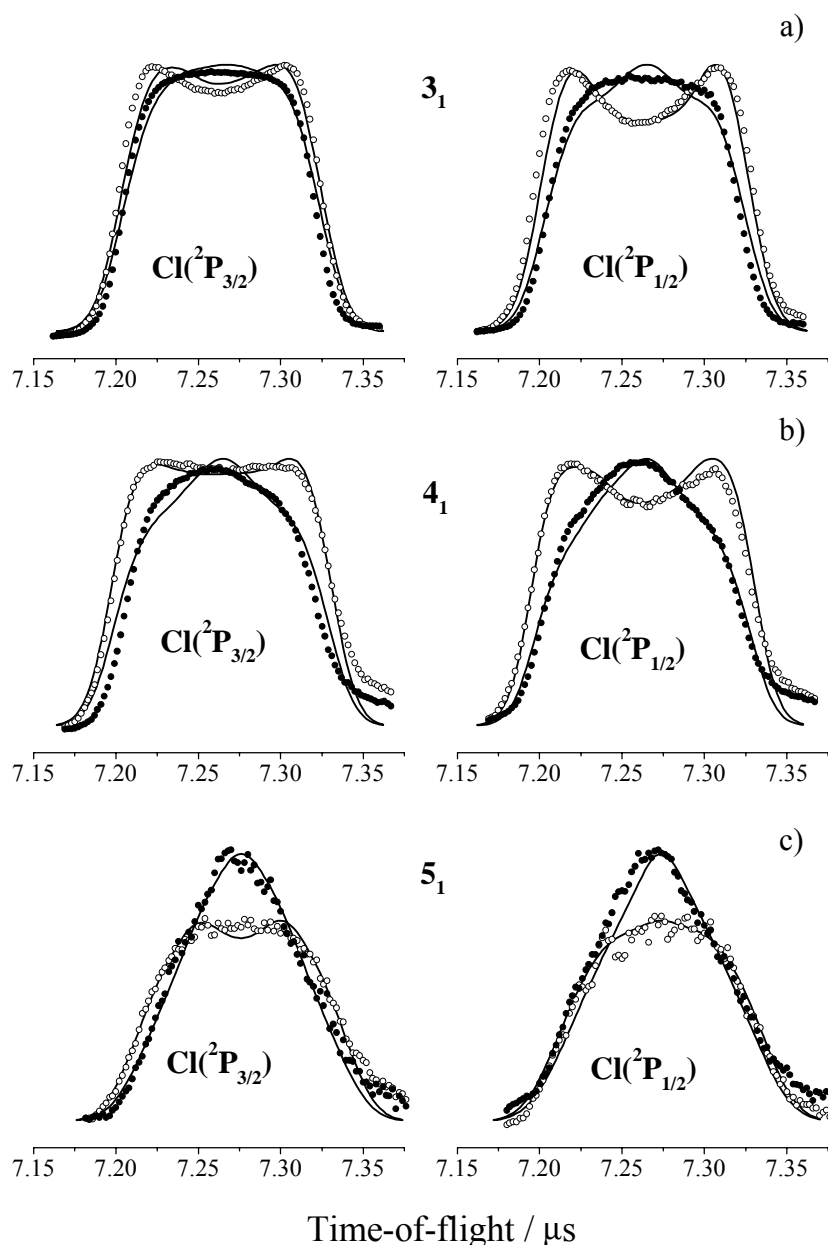


**Figure 7.3:** Arrival time distributions of  $\text{Cl}(^2\text{P}_{3/2})$  and  $\text{Cl}^*(^2\text{P}_{1/2})$  photofragments produced in the  $\sim 235$  nm photolysis of  $\text{CHFCl}_2$  pre-excited to the Q-branch of the  $3_1$  (panel a),  $4_1$  (panel b), and  $5_1$  (panel c) states. Open circles and solid points are experimental data points taken with the polarization of the UV photolysis/probe laser parallel and perpendicular, respectively, to the TOF MS axis. The polarization of the overtone excitation laser was perpendicular to the TOF MS axis. Solid lines are the simulations of the corresponding profiles. These lines denote the best fit velocity distributions, with constant  $\beta$ , finite time response of the apparatus (modeled as a Gaussian with 20 ns full-width-half-maximum) and Doppler selection by the finite bandwidth of the probe laser (modeled as  $0.3 \text{ cm}^{-1}$  at the 1-photon wavenumber).

The Cl and Cl\* photofragment spectra, shown in Fig. 7.3 (a) and 7.3 (b), indicate that the profiles are doubly peaked for the parallel polarization of the UV laser and singly peaked for the perpendicular one. The double peaks are due to the formation of Cl and Cl\* photofragments of equal translational energies but with velocity vectors pointing towards and opposite the flight axis. The shapes of the profiles indicate that both Cl and Cl\* photofragments are released predominantly through a parallel electronic transition with a positive  $\beta$ .<sup>27-29</sup> Also, from comparison of the profiles of Cl and Cl\* obtained in VMP via the intermediate state  $5_1$  to those via  $3_1$  and  $4_1$  it is evident that the intensities of the centers of the arrival time profiles increase and are much more pronounced in the former. This happens although the profiles were monitored under similar conditions, except the excitation wavelengths employed for the preparation of the  $5_1$ ,  $3_1$ , and  $4_1$  states. Therefore, the increase in the intensity of the center of the arrival time distribution can be attributed to an increase in production of Cl and Cl\* photofragments with nearly zero center of mass (c.m.) translational energies.

To extract quantitatively the  $\beta$  parameters and the c.m. Cl and Cl\* photofragment velocities, simulations of the TOF spectral profiles were carried out. In order to derive kinetic energy distributions (KEDs) from the measured TOF profiles, one first must calculate the corresponding speed distribution  $P(v)$ . The speed distribution can be obtained from integrating over the angular part of the fully three-dimensional velocity distribution  $P(v, \theta, \varphi)$  in the spherical coordinate system associated with the electric field vector of the dissociation laser:

$$P(v) = \iint v^2 \sin\theta \, d\theta \, d\varphi \, P(v, \theta, \varphi) \quad (7.1)$$

with  $P(v, \theta) = P(v)[1 + \beta(v)P_2(\cos\theta)]$ .  $\beta(v)$  is the (velocity-dependent) anisotropy parameter characterizing the spatial fragment distribution, ranging from -1 (perpendicular transition) to +2 (parallel transition), and  $P_2$  is the second Legendre polynomial:  $P_2(x) = \frac{1}{2}(3x^2 - 1)$ . The experimentally observed TOF profile  $P(\Delta t)$ , on the other hand, is proportional to the  $P(v_z)$  distribution of the velocity component  $v_z$  along the spectrometer axis  $z$ :

$$P(v_z) = \int_{v_z}^{\infty} dv \iint dv_y \, dv_x \, P(v; v_x, v_y, v_z) \delta(v - \sqrt{v_x^2 + v_y^2 + v_z^2}) \quad (7.2)$$

where the (xyz) Cartesian coordinate system is attached to the spectrometer axis defining z. The  $\delta$ -function only serves to satisfy the condition  $v^2 = v_x^2 + v_y^2 + v_z^2$ . Then, upon proper transformation of the coordinate systems, the experimentally observed TOF profile, represented by  $P(v_z)$ , and the desired KED, represented by  $P(v)$ , are related by:

$$P(v_z) = \int_{v_z}^{\infty} dv \left( \frac{P(v)}{2v} \left( 1 + \beta(v) P_2(\cos \frac{v_z}{v}) P_2(\cos \gamma) \right) \right) \quad (7.3)$$

where  $\gamma$  is the angle of the electric field vector of the dissociation laser with the spectrometer axis z. In general, this equation cannot analytically be inverted in order to obtain  $P(v)$  from  $P(v_z)$ . Often, the relationship between  $P(v)$  and  $P(v_z)$  is even more complicated. Especially for a large kinetic energy release the laser bandwidth  $\delta v_L$  is usually smaller than the Doppler width  $\Delta v_D$  of the absorption lines of the fragments, and the selective excitation of a fragment subset with small velocity components  $v_x$  along the laser beam axis must be considered. Then, the  $v_y$ -integration cannot be performed any more, and eq. (7.3) becomes:

$$P(v_z) = \int_{v_z}^{\infty} dv \int_{-\sqrt{v^2-v_z^2}}^{\sqrt{v^2-v_z^2}} dv_y P(v) \frac{L(v, v_y, v_z)}{\sqrt{v^2-v_y^2-v_z^2}} \left\{ 1 + \beta(v) P_2\left(\frac{v_y \sin \gamma + v_z \cos \gamma}{v}\right) \right\} \quad (7.4)$$

where  $L(v, v_y, v_z)$  contains the excitation probability for a narrow bandwidth laser ( $\delta v_L < \Delta v_D$ ). Moreover, the proportionality between  $v_z$  and  $\Delta t$  is affected by the instrument response function of the spectrometer, with which the  $P(v_z)$  velocity component distribution has to be convoluted. Therefore, we developed a robust forward convolution procedure based on a genetic algorithm where trial functions  $P(v)$  and  $\beta(v)$  are optimized with respect to eq. (7.4), i.e. taking into account all the above mentioned effects. Further details of the algorithm written by Dr. C. Maul (TU Braunschweig) will be published elsewhere. The best simulations obtained by the outlined procedure are shown as solid lines in Fig. 7.3. As can be seen, the fittings to the experimental data are very good, although only a single velocity-independent  $\beta$  parameter was employed for Cl or Cl\* photofragments.

### 7.3.2 Speed Distributions

The speed distributions,  $P(v)$ , for Cl and Cl\* photofragments resulting from VMP via the  $3_1$ ,  $4_1$ , and  $5_1$  states are shown in Fig. 7.4 (a) – (c).

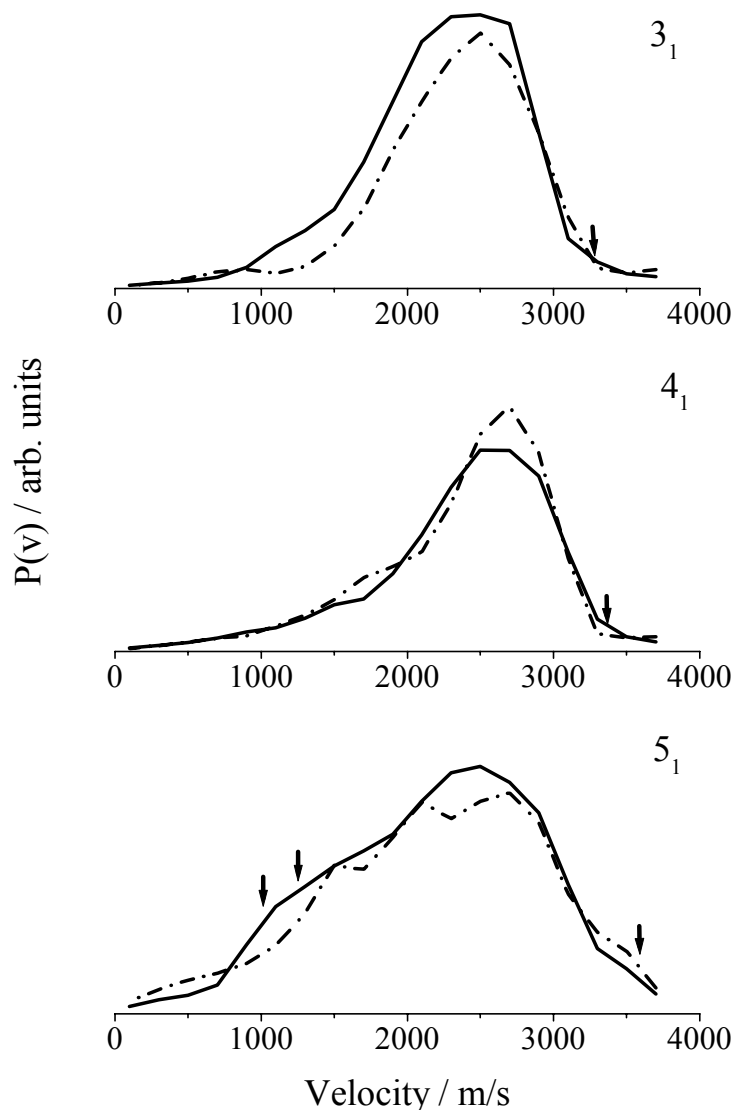
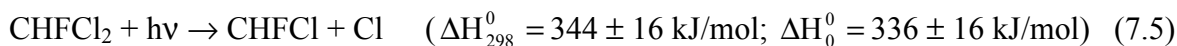
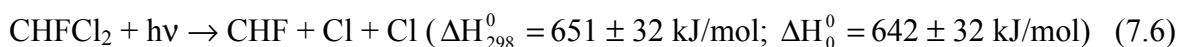


**Figure 7.4:** Velocity distributions of Cl ( $^2P_{3/2}$ ) (solid line) and Cl\* ( $^2P_{1/2}$ ) (dashed line) in  $\sim 235$  nm photodissociation of vibrationally excited  $\text{CHFCl}_2$   $3_1$ ,  $4_1$ , and  $5_1$ . The arrows at the high velocities, in the different panels, indicate the maximum possible velocities calculated for the two-body photodissociation of  $\text{CHFCl}_2$   $3_1$ ,  $4_1$ , and  $5_1$ , respectively. The other two arrows in the slow velocity region of the bottom panel indicate the maximum allowed velocity in the sequential and concerted three-body process, respectively.

In some cases the distributions suffer from some distortion, due to the binning of velocities during the simulation procedure. Nevertheless, it can clearly be seen that the top panel distributions of both Cl and Cl\* are significantly narrower than the bottom panel distribution corresponding to VMP of CHFCl<sub>2</sub> via the 5<sub>1</sub> state. It is also obvious that the broadening of the latter results from production of "faster" Cl and Cl\* photofragments, as well as slower Cl and Cl\*. The production of faster Cl and Cl\* photofragments arises from higher combined energies (IR/visible+UV) employed in the VMP of CHFCl<sub>2</sub> (5<sub>1</sub>) [ $\sim 56\,459\text{ cm}^{-1}$  (675 kJ/mol)] than in (4<sub>1</sub>) [ $\sim 53\,873\text{ cm}^{-1}$  (644 kJ/mol)] and (3<sub>1</sub>) [ $\sim 51\,236\text{ cm}^{-1}$  (612 kJ/mol)]. The combined energies in the VMP of CHFCl<sub>2</sub> (3<sub>1</sub>), (4<sub>1</sub>) and (5<sub>1</sub>) exceed that required for the loss of one chlorine atom,



but the first two do not surpass the threshold for the three-body process where two ground state chlorine atoms are released:



The enthalpies,  $\Delta H^0$ , of reactions (7.5) and (7.6) were calculated for the spin-orbit states with the lowest energy from the standard enthalpies of formation ( $\Delta H_f^0$ ) of the molecule and radicals involved in the process<sup>30,31</sup> and the errors were calculated as the sum of individual squared errors. The  $\Delta H^0$  required for loss of one or two Cl\* atoms is higher than the values given for one or two Cl atoms in reaction (7.5) and (7.6) by 10.6 kJ/mol and 21.2 kJ/mol, respectively.

Taking into account the combined energies channeled into CHFCl<sub>2</sub> molecules and assuming that  $\Delta H_0^0$  equals the C-Cl bond dissociation energy,  $D_0$ , the available energy,  $E_{av}$ , and the maximum energetically allowed velocities for Cl photofragments were calculated. The maximum Cl velocity arising from decay channel (7.5) is  $\sim 3220 \pm 90$  m/s for molecules pre-excited to the 3<sub>1</sub> state,  $\sim 3400 \pm 90$  m/s for those to the 4<sub>1</sub> state and  $\sim 3570 \pm 90$  m/s for those to the 5<sub>1</sub> state, as indicated by the arrows in Fig. 7.4. Also Fig. 7.4 clearly shows that the velocity distributions are centered at relatively high values

with tails that reach the maximum Cl velocities. The correspondence of the distribution centers to large velocities might indicate that the dissociation process occurs on a repulsive PES, as expected from the broad and unstructured first absorption band of CHFCl<sub>2</sub>.<sup>25</sup>

In addition, by converting the speed distributions obtained in VMP of CHFCl<sub>2</sub> (3<sub>1</sub>) and (4<sub>1</sub>) to translational energy distributions, the average translational energy  $\langle E_T \rangle$  release of the CHFCl + Cl fragment pair via reaction (7.5) could be calculated. The  $\langle E_T \rangle$  for VMP of CHFCl<sub>2</sub> (3<sub>1</sub>) and (4<sub>1</sub>) is 126 and 141 kJ/mol, respectively. Since the excess of  $E_{av}$ , 276 kJ/mol for (3<sub>1</sub>) and 308 kJ/mol for (4<sub>1</sub>), is imparted into internal and translational energies of the fragments, it is deduced that 150 and 167 kJ/mol remain as internal energies of the CHFCl in VMP of CHFCl<sub>2</sub> (3<sub>1</sub>) and (4<sub>1</sub>), respectively. Also, the translational energy disposal fraction,  $\langle E_T \rangle / E_{avl}$ , was calculated to be 0.46 for 235 nm photodissociation of CHFCl<sub>2</sub> (3<sub>1</sub>) and (4<sub>1</sub>). Comparison of this value to that obtained directly in the PTS experiments of Huber and co-workers<sup>21</sup> in 193 nm photodissociation of vibrationless ground state CHFCl<sub>2</sub> (0.44) shows an excellent agreement. Our value is also quite close to those measured for the 193 nm photolysis of other chloromethanes releasing Cl photofragments, including: CHCl<sub>3</sub> [0.43 (Ref. 21) and 0.41 (Ref. 32)], CF<sub>2</sub>Cl<sub>2</sub> [0.50 (Ref. 32) and 0.47 (Ref. 33)], CFC<sub>3</sub> [0.43 (Ref. 32) and 0.47 (Ref. 34)] and CCl<sub>4</sub> [0.35 (Ref. 32)]. This implies that a rather high kinetic energy release occurs in the photodissociation of vibrationally excited CHFCl<sub>2</sub> similarly to the photodissociation of vibrationless ground state molecules agreeing with a direct dissociation process on a repulsive surface. It is worth noting that, as stated by Huber<sup>21</sup> and by Gentry<sup>32</sup> and their co-workers, their translational energy disposal fraction and also ours differ from those obtained by Matsumi et al.<sup>35</sup> They probed the Cl atoms by REMPI and measured the Doppler profiles in 193 nm photodissociation of several chloromethanes. The  $\langle E_T \rangle / E_{av}$  that they obtained were much higher, i.e., 0.85 for CHCl<sub>3</sub> and 0.78 for CH<sub>3</sub>Cl.

The slower Cl and Cl\* photofragments, observed in the VMP of CHFCl<sub>2</sub> (5<sub>1</sub>) might emerge from the synchronous concerted three-body decay, where two C-Cl bonds are broken simultaneously, or from sequential three-body decay.<sup>17,18</sup> For the former the maximum allowed Cl velocity is 970 m/s and for the latter 1100 m/s, as indicated by the corresponding arrows of the bottom panel of Fig. 7.4. Assuming that all the slow Cl atoms are formed in the three-body process, the upper limit of their fraction can be estimated as 6 % for the synchronous concerted and 10 % for the sequential three-body decay. It is

noteworthy that the calculated maximum velocities, based on the above enthalpies for reaction, suffer from inaccuracies due to the relatively large uncertainties in the enthalpies. Relying on the observed velocity distribution, it is difficult to evaluate the contribution of each of the three-body decay processes, however, it is anticipated that the slow Cl and Cl\* photofragments are formed via C-Cl bond ruptures. An additional possibility that has to be considered is that of release of H atom first ( $\Delta H_{298}^0 = 414$  kJ/mol) followed by release of Cl and Cl\* ( $\Delta H_{298}^0 = 604$  kJ/mol). However, since the first step is not too efficient,<sup>16</sup> it seems unlikely that the slow Cl and Cl\* will result from this pathway. Moreover, it does not seem reasonable that the slow Cl and Cl\* are not observed in VMP of CHFCl<sub>2</sub> pre-excited to the 4<sub>1</sub> state that provides a combined energy of 644 kJ/mol, above the one needed for this pathway.

### 7.3.3 Anisotropies

The recoil anisotropies derived from the profiles might also provide some information regarding the mechanism of bond breaking. The retrieved  $\beta$  parameters indicate that the Cl and Cl\* arising from  $\sim 235$  nm photodissociation of CHFCl<sub>2</sub> (3<sub>1</sub>), (4<sub>1</sub>), and (5<sub>1</sub>) via two- (7.5) or three-body (7.6) processes possess positive anisotropies, lower than the limiting values. The  $\beta$  parameters of Cl increase somewhat with increasing combined energy, rising from  $\beta = 0.14 \pm 0.05$  to  $0.27 \pm 0.06$ , and to  $0.47 \pm 0.07$ , while those of Cl\* are nearly constant with values of  $\beta = 0.36 \pm 0.06$ ,  $0.43 \pm 0.05$ , and  $0.34 \pm 0.04$ . Errors were calculated from the scattering of the 10 "best"  $\beta$  parameters obtained by the data analysis procedure described above.

As mentioned above, the magnitude and sign of  $\beta$  are related to the orientation of the transition dipole moment,  $\mu$ , in the parent molecule, the symmetry of the excited state and the excited state lifetime. The theoretical limit for the  $\beta$  parameter, with  $\mu$  parallel to the line connecting the two Cl atoms, was calculated by Huber and co-workers<sup>21</sup> and estimated to be  $\sim 1.1$  (based on a Cl-C-Cl bond angle of 112° in CHFCl<sub>2</sub>). They obtained  $\beta$  of  $0.5 \pm 0.1$  in 193 nm photodissociation of CHFCl<sub>2</sub>, indicating a partial loss of anisotropy. This loss was attributed either to a geometrical rearrangement during dissociation or to a

small contribution of an electronic transition of  $A' \leftarrow A'$  symmetry overlapping the dominant  $A'' \leftarrow A'$  transition.

The  $\beta$  values obtained in the VMP experiment are also positive, presumably due to the access of similar upper electronic states as in 193 nm photodissociation. The  $\text{CHFCl}_2$  molecule belongs to the  $C_s$  symmetry group, for identical chlorine isotopes, and it is anticipated that  $A'$  and  $A''$  transitions are also involved in the absorption from the vibrationally excited state. Indeed, calculations by Ying and Leung<sup>36</sup> have shown that two transitions of  $A''$  and two of  $A'$  symmetry underlie the first absorption band of  $\text{CHFCl}_2$ , related to the  $\sigma^* \leftarrow n$  transition, and that the predominant contribution rises from the lowest energy  $A''$  transition and some from one of the  $A'$ . Relying on the accessibility of the upper dissociative states it is conceivable that the dissociation is prompt and it does not seem that the rotational motion accounts for the reduction of  $\beta$  from its limiting value. Consequently, the observation of less than limiting  $\beta$  values emerge from dynamical factors. From the measured  $\beta$ , it is inferred that both Cl and  $\text{Cl}^*$  are produced as a result of simultaneous absorption to both  $A''$  and  $A'$  states, that mix probably via curve crossing to release Cl and  $\text{Cl}^*$ . Also, due to the increase of the  $\beta$  corresponding to Cl, it is likely that the contribution of the  $A''$  state to this channel increases with increasing combined energy. Relying on our observation that in  $\sim 235$  nm photodissociation of vibrationally excited  $\text{CHFCl}_2$  ( $3_1$ ) and ( $4_1$ ) the yield of  $\text{Cl}^*$  photofragments was about half that of Cl, we already suggested that probably two states are involved.<sup>16</sup> However, the new findings contrast our suggestion that preferential Cl formation rises from a predominant  $A''$  transition that proceeded adiabatically to ground state chlorine, and that of  $\text{Cl}^*$  from the  $A'$  state that correlates with it directly or via nonadiabatic crossing. Absorption via several transitions and curve crossings were suggested to account for the observed branching ratios or the anisotropies in other halocarbons as well, including  $\text{CH}_3\text{Cl}$  and  $\text{CHD}_2\text{Cl}$ ,<sup>12</sup>  $\text{CH}_2\text{BrCl}$ ,<sup>37</sup>  $\text{CH}_3\text{I}$ ,<sup>38,39</sup>  $\text{CF}_3\text{I}$ ,<sup>40</sup>  $\text{CH}_2\text{I}_2$ ,<sup>41</sup>  $\text{CF}_2\text{I}_2$ .<sup>42</sup>

The observed increase in the Cl channel anisotropy in VMP of  $\text{CHFCl}_2$  molecules promoted from  $5_1$  relative to those from  $4_1$  and  $3_1$  is a hint for a concerted three-body decay. In case of sequential three-body decay one would expect a lower  $\beta$  parameter than in the two-body case due to the increased dissociation lifetime. Relying on the observation of the increase in  $\beta$  it seems likely that the concerted three-body decay is responsible for

the slow Cl. As for  $\text{Cl}^*$  photofragments, due to the decrease in  $\beta$  in VMP of  $\text{CHFCl}_2$  ( $5_1$ ) relative to that in ( $4_1$ ) it might be that a sequential three-body decay is also involved. A similar behavior was observed in the photodissociation of  $\text{CF}_2\text{I}_2$ <sup>41</sup> and of  $\text{CF}_2\text{Br}_2$ .<sup>43</sup> For  $\text{CF}_2\text{I}_2$ , a smooth transition took place from a single two-body decay to a sequential three-body decay and finally to a concerted three-body decay upon increasing the energy of the dissociating photon.

## 7.4 Conclusions

The VMP of  $\text{CHFCl}_2$  pre-excited to the  $3_1$ ,  $4_1$ , and  $5_1$  C-H polyad components was studied using the REMPI-TOF technique for measurement of time-of-arrival profiles for the Cl and  $\text{Cl}^*$  photofragments. The data analysis yielded the photofragments velocity distributions and the recoil anisotropy parameters. These results suggest that the photodissociation of  $\text{CHFCl}_2$  ( $3_1$ ) and ( $4_1$ ) occurs only via two-body decay while that of  $\text{CHFCl}_2$  ( $5_1$ ) via both two- and three-body decays. In the two-body decay, the translational energy release into the fragments is quite high (~45 % of the available energy) and excellently agrees with that found in 193 nm photodissociation of vibrationless ground state  $\text{CHFCl}_2$ . The evidence for three-body decay comes from the slow tail observed in the velocity distributions of Cl and  $\text{Cl}^*$  appearing when the combined energy of vibrational and electronic excitations overcome the dissociation barrier. The anisotropy parameters are lower than the limiting values indicating that more than one PES is involved in the excitation and also that both Cl and  $\text{Cl}^*$  are released from both of them. Due to the similarity of the anisotropy parameters obtained for Cl in the two- and three-body decays, it is deduced that the latter one is concerted, while for  $\text{Cl}^*$  it could be both sequential and concerted. Additional studies that will further examine the internal parent excitation effect on the three-body bond breakup are needed.

## 7.5 Acknowledgment

We are grateful to Prof. P. J. Dagdigian and Dr. A. Melchior for useful discussions and for a critical reading of the manuscript. This research was supported by the German-Israeli Foundation (GIF) under grant No. I 0537-098.05/97 and by the James Franck Binational

---

German-Israeli Program in Laser-Matter Interaction. T. E. gratefully acknowledges financial support from the Fonds der Chemischen Industrie and the Minerva Foundation.

---

- <sup>1</sup> F. F. Crim, *J. Phys. Chem.* **100**, 12725 (1996); and references therein.
- <sup>2</sup> D. Hausler, P. Andresen, and R. Schinke, *J. Chem. Phys.* **87**, 3949 (1987); V. Engel, V. Steammmler, R.L. Van der Wal, F. F. Crim, R. J. Sension, B. J. Hudson, P. Andresen, S. Hennig, K. Weide, and R. Schinke, *J. Phys. Chem.* **96**, 3201 (1992).
- <sup>3</sup> R. L. Van der Wal, J. L. Scott, and F. F. Crim, *J. Chem. Phys.* **92**, 803 (1990); R. L. Van der Wal, J. L. Scott, and F. F. Crim, *J. Chem. Phys.* **94**, 1859 (1991).
- <sup>4</sup> I. Bar, Y. Cohen, D. David, S. Rosenwaks, and J. J. Valentini, *J. Chem. Phys.* **93**, 2146 (1990); I. Bar, Y. Cohen, D. David, T. Arusi-Parpar, S. Rosenwaks, and J. J. Valentini, *J. Chem. Phys.* **95**, 3341 (1991); D. David, A. Strugano, I. Bar, and S. Rosenwaks, *J. Chem. Phys.* **98**, 409 (1993); I. Bar, D. David, and S. Rosenwaks, *Chem. Phys.* **187**, 21 (1994).
- <sup>5</sup> M. Brouard and S. R. Langford, *J. Chem. Phys.* **106**, 6354 (1997).
- <sup>6</sup> Y. Cohen, I. Bar, and S. Rosenwaks, *J. Chem. Phys.* **102**, 3612 (1995); Y. Cohen, I. Bar and S. Rosenwaks, *Chem. Phys. Lett.* **228**, 426 (1994).
- <sup>7</sup> E. Woods III, H. L. Berghout, C. M. Cheatum, and F. F. Crim, *J. Phys. Chem. A* **104**, 10356 (2000); M. J. Coffey, H. L. Berghout, E. Woods III, and F. F. Crim, *J. Chem. Phys.* **110**, 10850 (1999).
- <sup>8</sup> J. Zhang, C. W. Riehn, M. Dulligan, and C. Wittig, *J. Chem. Phys.* **103**, 6815 (1995).
- <sup>9</sup> R. P. Schmid, T. Arusi-Parpar, R.-J. Li, I. Bar, and S. Rosenwaks, *J. Chem. Phys.* **107**, 385 (1997); R. P. Schmid, Y. Ganot, I. Bar, and S. Rosenwaks, *J. Chem. Phys.* **109**, 8959 (1998).
- <sup>10</sup> R. P. Schmid, Y. Ganot, I. Bar, and S. Rosenwaks, *J. Molec. Struct.* **197**, 480 (1999); T. Arusi-Parpar, R. P. Schmid, R.-J. Li, I. Bar, and S. Rosenwaks, *Chem. Phys. Lett.* **268**, 163 (1997).
- <sup>11</sup> X. Chen, Y. Ganot, I. Bar, and S. Rosenwaks, *J. Chem. Phys.* **113**, 5134 (2000); Y. Ganot, R. Marom, I. Bar, and S. Rosenwaks, in preparation.
- <sup>12</sup> H. M. Lambert and P. J. Dagdigian, *J. Chem. Phys.* **109**, 7810 (1998); H. M. Lambert and P. J. Dagdigian, *Chem. Phys. Lett.* **275**, 499 (1997); A. Melchior, H. M. Lambert, P. J. Dagdigian, I. Bar, and S. Rosenwaks, *Isr. J. Chem.* **37**, 455 (1997).
- <sup>13</sup> R. J. Barnes, A. Sinha, P. J. Dagdigian, and H.M. Lambert, *J. Chem. Phys.* **111**, 151 (1999).
- <sup>14</sup> A. Melchior, X. Chen, I. Bar, and S. Rosenwaks, *Chem. Phys. Lett.* **315**, 421 (1999).
- <sup>15</sup> A. Melchior, X. Chen, I. Bar, and S. Rosenwaks, *J. Chem. Phys.* **112**, 10787 (2000).
- <sup>16</sup> A. Melchior, X. Chen, I. Bar, and S. Rosenwaks, *J. Phys. Chem. A* **104**, 7927 (2000).
- <sup>17</sup> C. Maul and K.-H. Gericke, *J. Phys. Chem. A* **104**, 2531 (2000).
- <sup>18</sup> C. Maul and K.-H. Gericke, *Int. Rev. Phys. Chem.* **16**, 1 (1997).
- <sup>19</sup> R. E. Rebbert, S. G. Lias and P. Ausloos, *J. Photochem.* **8**, 17 (1978).
- <sup>20</sup> S. Hauteclouque, *J. Photochem.* **12**, 197 (1980).
- <sup>21</sup> X. Yang, P. Felder, and J. R. Huber, *Chem. Phys.* **189**, 127 (1994).

- 
- <sup>22</sup> H.-R. Dubal and M. Quack, *J. Chem. Phys.* **81**, 3779 (1984).
- <sup>23</sup> W.C. Wiley and I. H. McLaren, *Rev. Sci. Instrum.* **25**, 1150 (1981).
- <sup>24</sup> R. Liyanage, Y. Yang, S. Hashimoto, R. J. Gordon, and R. Field, *J. Chem. Phys.* **103** (1995) 6811.
- <sup>25</sup> C. Hubrich, C. Zetzsech, and F. Stuhl, *Ber. Bunsen. Ges. Phys. Chem.* **81**, 437 (1977).
- <sup>26</sup> D. F. Varley and P. J. Dagdigian, *J. Phys. Chem.* **99**, 9843 (1995).
- <sup>27</sup> R. N. Zare, *Mol. Photochem.* **4**, 1 (1972).
- <sup>28</sup> G. E. Hall and P. L. Houston, *Annu. Rev. Phys. Chem.* **40**, 375 (1989).
- <sup>29</sup> R. J. Gordon and G. E. Hall, *Adv. Chem. Phys.* **96**, 1 (1996).
- <sup>30</sup> H. Y. Afeefy, J. F. Liebman, and S. E. Stein, "Neutral Thermochemical Data" in NIST Chemistry WebBook, NIST Standard Reference Database Number 69, Eds. W.G. Mallard and P. J. Linstrom, February 2000, National Institute of Standards and Technology, Gaithersburg MD, 2089 (<http://webbook.nist.gov>).
- <sup>31</sup> E. Tschuikow-Roux and S. Paddison, *Intern. J. Chem. Kinet.* **19**, 15 (1987).
- <sup>32</sup> M. D. Nachbor, C. F. Giese, and W. R. Gentry, *J. Phys. Chem.* **99**, 15400 (1995).
- <sup>33</sup> G. Baum and J. R. Huber, *Chem. Phys. Lett.* **203**, 261 (1993).
- <sup>34</sup> P. Felder and C. Demuth, *Chem. Phys. Lett.* **208**, 21 (1993).
- <sup>35</sup> Y. Matsumi, K. Tonokura, M. Kawasaki, G. Inoue, S. Satyapal, and R. Bersohn, *J. Chem. Phys.* **94**, 2669 (1991); *ibid.* **97**, 5261 (1992).
- <sup>36</sup> J. F. Ying and K. T. Leung, *J. Chem. Phys.* **105**, 2188 (1996).
- <sup>37</sup> W. S. McGivern, R. Li, P. Zou, and S. W. North, *J. Chem. Phys.* **111**, 5771 (1999); P. Zou, S. McGivern, and S. W. North, *Phys. Chem. Chem. Phys.* **2**, 3785 (2000)
- <sup>38</sup> R. Orgorzalek Loo, H.-P. Haerri, G. E. Hall, and P. L. Houston, *J. Chem. Phys.* **90**, 4222 (1989).
- <sup>39</sup> M. D. Person, P. W. Kash, and L. J. Butler, *J. Chem. Phys.* **94**, 2557 (1991).
- <sup>40</sup> A. Furlan, T. Gejo, and R. J. Huber, *J. Phys. Chem.* **100**, 7956 (1996).
- <sup>41</sup> J. B. Koeffend and S. R. Leone, *Chem. Phys. Lett.* **81**, 136 (1981).
- <sup>42</sup> E. A. J. Wannemacher, P. Felder, and J. R. Huber, *J. Chem. Phys.* **95**, 986 (1991), G. Baum, P. Felder, and J. R. Huber, *J. Chem. Phys.* **98**, 1999 (1993). K. Bergmann, R. T. Carter, G. E. Hall, and J. R. Huber, *J. Chem. Phys.* **109**, 474 (1998); W. Radloff, P. Farmana, V. Stert, E. Schreiber, and J. R. Huber, *Chem. Phys. Lett.* **291**, 173 (1998); H. A. Scheld, A. Furlan, and J. R. Huber, *Chem. Phys. Lett.* **326**, 366 (2000).
- <sup>43</sup> M. R. Cameron, S. A. Jones, G. F. Metha, and S. H. Kable, *Phys. Chem. Chem. Phys.* **2**, 2539 (2000).